1 Numerical Simulation of the Muon Collider Target

The numerical simulation of hydro- and magnetohydrodynamics processes in the Muon Collider target is needed for better understanding of the physics involved and for answering engineering design questions. The muon collider target will contain a series of mercury jet pulses of about 0.5 cm in radius and 60 cm in length. Each pulse will be shot at a velocity of 30-35 m/sec into a 20 Tesla magnetic field at a small angle (0.1 rad) to the axis of the field. When the jet reaches the center of the magnet, it is hit with 3 ns proton pulses arriving with 20 ms time period; each proton pulse will deposit about 100 J/g of energy in the mercury.

The main issues of the target design addressed in our numerical studies are the distortion of the jet due to eddy currents as it propagates through the magnetic coil, the deformation of the jet surface due to strong pressure waves caused by the proton pulses and the probability of the jet breakup. Studying the state of the target during its interaction with proton pulses will help to achieve the maximal proton production rate and therefore an optimal target performance.

1.1 Magnetohydrodynamics of Free Surface Liquid Flows

The basic set of equations describing the interaction of a compressible conducting fluid flow and a magnetic field is contained in Maxwell's equations and in the equations of fluid dynamics suitably modified [1, 11]. Namely, the systems contains the mass, momentum and energy conservation equations for the fluid which have hyperbolic nature and a parabolic equation for the evolution of the magnetic field.

$$
\begin{aligned}
\frac{\partial \rho}{\partial t} &= -\nabla \cdot (\rho \mathbf{u}), && (1)\\
\rho \left(\frac{\partial}{\partial t} + \mathbf{u} \cdot \nabla \right) \mathbf{u} &= -\nabla P + \rho \mathbf{X} + \frac{1}{c}(\mathbf{J} \times \mathbf{B}), && (2)\\
\rho \left(\frac{\partial}{\partial t} + \mathbf{u} \cdot \nabla \right) U &= -P \nabla \cdot \mathbf{u} + \frac{1}{\sigma}\mathbf{J}^2 - \frac{1}{c}\mathbf{u} \cdot (\mathbf{J} \times \mathbf{B}), && (3)\\
\frac{\partial \mathbf{B}}{\partial t} &= \nabla \times (\mathbf{u} \times \mathbf{B}) - \nabla \times (\frac{c^2}{4\pi\sigma} \nabla \times \mathbf{B}), && (4)\\
\nabla \cdot \mathbf{B} &= 0, && (5)
\end{aligned}
$$

Here $\mathbf{u}$, ρ and U are the velocity, density and total energy of the fluid, respectively, P is the total stress tensor, $\mathbf{X}$ includes external forces of nonmagnetic origin, $\mathbf{B}$ is the magnetic field induction, $\mathbf{J}$ is the current density distribution and σ is the fluid conductivity. The magnetic field $\mathbf{H}$ and magnetic induction $\mathbf{B}$ are related by the magnetic permeability coefficient μ: $\mathbf{B} = \mu\mathbf{H}$.

The system (1-4) must be closed with an equation of state. We are especially interested in fluid behavior under extreme thermodynamics conditions. Some related equation of state models are discussed below.

The following boundary conditions must be satisfied at the jet surface:

i) the normal component of the velocity field is continuous across the material interface.

ii) the normal and tangential components of the magnetic field at the material interface are related as

$$\mathbf{n} \cdot (\mathbf{B}_2 - \mathbf{B}_1) = 0, \tag{6}$$

$$\mathbf{n} \times (\mathbf{H}_2 - \mathbf{H}_1) = \frac{4\pi}{c}\mathbf{K}, \tag{7}$$

where $\mathbf{K}$ is the surface current density. The above jump conditions define the refraction of magnetic lines on the material interface. We can assume $\mu = 1$ for most fluids. Notice that the surface current density $\mathbf{K}$ corresponds to a current localized in a thin fluid boundary layer (δ-functional current) which is non-zero only for superconducting materials. The current density in fluids at normal conditions is distributed in the 3D volume and $\mathbf{K} = 0$. Therefore, the equations (6,7) simply require the continuity of the normal and tangential components of the magnetic field.

The behavior of a fluid in the presence of electromagnetic fields is governed to a large extent by the magnitude of the conductivity. For fluid at rest (4) reduces to the diffusion equation

$$\frac{\partial \mathbf{B}}{\partial t} = \frac{c^2}{4\pi\mu\sigma}\Delta\mathbf{B} \tag{8}$$

This means that an initial configuration of magnetic field will decay with typical diffusion time

$$\tau = \frac{4\pi\mu\sigma L^2}{c^2},$$

where L is a characteristic length of the spatial variation of $\mathbf{B}$. Despite being good enough conductors, most of liquid metals including mercury are characterized by small diffusion times (33 microseconds for a mercury droplet of 1 cm radius) compared to some solid conductors (1 sec for a copper sphere of 1 cm radius). Therefore the magnetic field penetration in such liquid conductors can be considered as an instantaneous process.

Another crucial phenomena for MHD flows of compressible conducting fluids is the propagation of Alfven waves. For mercury at room temperature the Alfven velocity

$$\mathbf{v}_A = \frac{\mathbf{B}_0}{\sqrt{4\pi\rho_0}},$$

where $\mathbf{B}_0$ and ρ_0 are unperturbed (mean) values of the magnetic induction and density of the fluid, respectively, is $[B_0(\mathrm{Gauss})/13.1]$ cm/sec. This is a small number compared with the speed of sound of 1.45×10^5 cm/sec even for the magnetic field of 20 T. In many cases, however, it is not desirable to compute Alfven waves explicitly in the system. If, in addition, both the magnetic field diffusion time and the eddy current induced magnetic field are small, an assumption of the constant in time magnetic field can be made. The current density distribution can be obtained in this case using Ohm's law

$$\mathbf{J} = \sigma\left(-\mathrm{grad}\phi + \frac{1}{c}\mathbf{u}\times\mathbf{B}\right). \tag{9}$$

Here ϕ is the electric field potential. The potential ϕ satisfies the following Poisson equation

$$\Delta\phi = \frac{1}{c}\mathrm{div}(\mathbf{u}\times\mathbf{B}), \tag{10}$$

and the Neumann boundary conditions

$$\left.\frac{\partial\phi}{\partial\mathbf{n}}\right|_{\Gamma} = \frac{1}{c}(\mathbf{u}\times\mathbf{B})\cdot\mathbf{n},$$

where $\mathbf{n}$ is a normal vector at the fluid boundary Γ. This approach is applicable for the study of a liquid metal jet moving in a magnetic field.

We shall use also the following simplification for the modeling of a thin jet moving along the solenoid axis. Let us consider a ring of liquid metal of radius r that is inside a thin jet moving with velocity u_z along the axis of a solenoid magnet. The magnetic flux $\Phi = \pi r^2 B_z$ through the ring varies with time because the ring is moving through the spatially varying magnetic field, and because the radius of the ring is varying at rate $u_r = dr/dt$. Therefore, an azimuthal electric field is induced around the ring:

$$\begin{aligned} 2\pi r E_\phi = -\frac{1}{c}\frac{d\Phi}{dt} &= -\frac{\pi r^2}{c}\frac{dB_z}{dt} - \frac{2\pi r u_r B_z}{c} \\ &= -\frac{\pi r^2 u_z}{c}\frac{\partial B_z}{\partial z} - \frac{2\pi r u_r B_z}{c}. \end{aligned}$$

This electric field leads to an azimuthal current density

$$J_\phi = \sigma E_\phi = -\frac{\sigma r u_z}{2c}\frac{\partial B_z}{\partial z} - \frac{\sigma u_r B_z}{c}, \tag{11}$$

which defines the Lorentz force in the momentum equation (2) and leads to the distortion of the jet moving in a non-uniform magnetic field.

The linear stability analysis of thin conducting liquid jets moving along the axis of a uniform magnetic field [1] and the corresponding analysis for the Muon Collider target [7] show that an axial uniform field tends to stabilize the jet surface. The influence of a strong nonuniform field must be studied by means of the numerical simulation.

1.2 Numerical Implementation

In this section, we shall describe numerical ideas implemented in the FronTier MHD code. FronTier represents interfaces as lower dimensional meshes moving through a volume filling grid [5]. The traditional volume filling finite difference grid supports smooth solutions located in the region between interfaces. The location of the discontinuity and the jump in the solution variables are defined on the lower dimensional grid or interface. The dynamics of the interface comes from the mathematical theory of Riemann solutions, which is an idealized solution of a single jump discontinuity for a conservation law. Where surfaces intersect in lower dimensional objects (curves in three dimensions), the dynamics is defined by a theory of higher dimensional Riemann problems such as the theory of shock polars in gas dynamics. Nonlocal correlations to these idealized Riemann solutions provide the coupling between the values on these two grid systems.

The computation of a dynamically evolving interface requires the ability to detect and resolve changes in the topology of the moving front. A valid interface is one where each surface and curve is connected, surfaces only intersect along curves and curves only intersect at points. We say that such an interface is untangled. Two independent numerical algorithms, grid-based tracking and grid-free tracking, were developed [5, 6] to resolve the untangling problem for the moving interface. The advantages and deficiencies of the two methods are complementary and an improved algorithm combining them into a single hybrid method was implemented in the FronTier code and described in [6].

We solve the hyperbolic subsystem of the MHD equations, namely the equations (1-3), on a finite difference grid in both domains separated by the free surface using FronTier's interface tracking numerical techniques.

Some features of the FronTier hyperbolic solvers include the use of high resolution methods such as MUSCL, Godunov and Lax-Wendroff with a large selection of Riemann solvers such as the exact Riemann solver, the Colella-Glaz approximate Riemann solver, the linear US/UP fit (Dukowich) Riemann solver, and the Gamma law fit. We use realistic models for the equation of state such as the polytropic and stiffened polytropic equation of state, the Gruneisen equation of state, and the SESAME tabular equation of state.

The evolution of the free fluid surface is obtained through the solution of the Riemann problem for compressible fluids [5, 13]. Notice that since we are primarily interested in the contact discontinuity propagation, we do not consider the Riemann problem for the MHD system and therefore neglect elementary waves typical for MHD Riemann solutions.

We have developed the following numerical approaches for solving the equation (4) for the magnetic field evolution and the Poisson equation (10):

Finite defference solvers based on regular grids. We have developed a parallel elliptic solver for the current density distribution equation (refeq10) based on finite difference technique on rectangular grid in regular domains. We have performed smoothening of discontinuities of physics fields and applied the cubic spline interpolation of the fields within several grid blocks. The corresponding parallel iterative solvers for linear systems of equations explore different Krylov subspace and preconditioning methods and are based on PETSC libraries [14]. The solver is very effective for modeling miltifluid MHD phenomena for fluids with smooth interfaces without small length scale perturbations. For MHD flows with unstable interfaces, we use FE solvers on meshes dynamically conforming to evolving interfaces.

Finite element solvers. Finete element solvers are based on grids dynamically conforming to the moving interface. The grid generation method is based on the point-shifted grid technique of McBryan [12]. For the elliptic and parabolic systems considered here we favor the mixed-hybrid finite element formulation of Chavent and Jaffre [2]. We utilize Glowinski-Wheeler domain decomposition [8]. The linear systems obtained for the subdomain "interior problems" are solved using direct methods which preconditioned conjugate gradients for the global "wire basket" problem. Preconditioners such as vector probing and balancing are used.

1.3 Modeling Thermodynamics Properties of Fluids

Material properties strongly influence the structure and dynamics of waves in any continuous mechanical system. In particular, elementary waves in

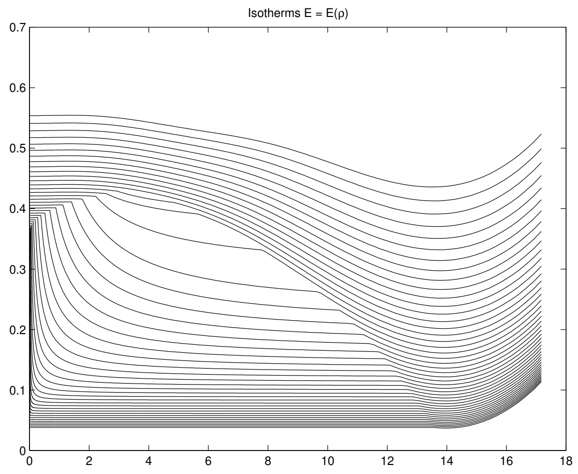

Figure 1: Isoterms of mercury specific internal energy as a function of density in the mixed liquid - vapor domain.

compresible fluids defined by Riemann problems depend both quantitatively and qualitatively on the property of an EOS.

SESAME equation of state for mercury. To model accurately the interaction of the mercury target with proton pulses, we created a tabulated equation of state for mercury in a wide temperature - pressure domain which includes the liquid-vapor phase transition and the critical point. The FronTier code uses SESAME Equation-of-Setate Library [9], developed at Los Alamos National Laboratory, to work with such tabulated eos format. Necessary data describing thermodynamic properties of mercury were obtained courtesy of T. Trucano of Sandia National Laboratory. The behavior of isotherms of the specific internal energy, pressure and entropy of mercury obtained using this equation of state are shown in Figures 1 - 3. The computational domain included the two phase region for mercury and the critical point.

Isentropic EOS for cavitating flows. The tabulated eos model allows an accurate description of equilibrium thermodynamic processes in mercury. However processes which occur in the mercury jet interacting with proton pulses go beyond the assumptions of equilibrium thermodynamics. Namely a regions of negative pressure (liquid tension) appear during the interaction which lead to the formation of cavities. To resolve such problem of negative pressures, we have developed an analytic two phase eos model for an isentropic regime of the flow. The model is based on the polytropic eos for

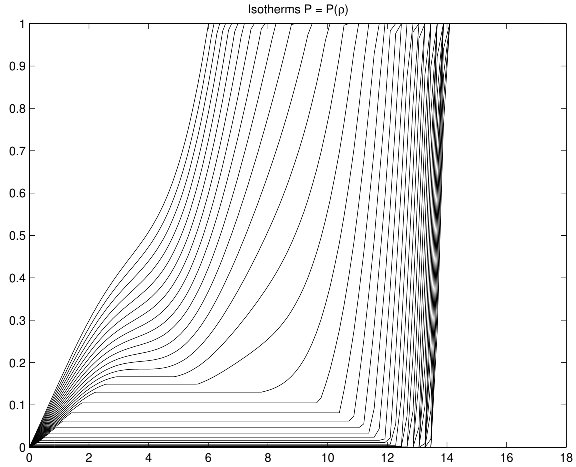

Figure 2: Isoterms of mercury pressure as a function of density in the mixed liquid - vapor domain.

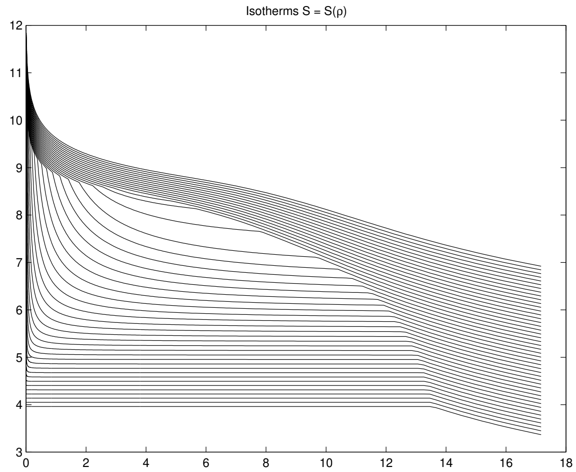

Figure 3: Isoterms of mercury entropy as a function of density in the mixed liquid - vapor domain.

the gas phase, the stiffened polytropic eos for the liquid phase [13] and the following eos type model (pressure - density relation):

$$P = P_l^{sat} + P_{gl}\log\left[\frac{\rho_g a_g^2(\rho_l + \alpha(\rho_g - \rho_l))}{\rho_l(\rho_g a_g^2 - \alpha(\rho_g a_g^2 - \rho_l a_l^2))}\right], \tag{12}$$

where

$$P_{gl} = \frac{\rho_g a_g^2 \rho_l a_l^2(\rho_g - \rho_l)}{\rho_g^2 a_g^2 - \rho_l^2 a_l^2},$$

Here ρ_g, p_g, a_g, ρ_l, p_l, a_l are the density, pressure, and sound speed of the saturated gas and liquid respectively, and the void fraction α is

$$\alpha = \frac{\rho - \rho_l}{\rho_g - \rho_l}.$$

We have developed the corresponding software library for FronTier.

1.4 Numerical Simulation Results

MHD studies of the Muon Collider target We shall present here numerical simulation results of thin jets of conducting fluid moving in highly nonuniform magnetic fields. In this numerical experiment, a 1 cm radius liquid jet is sent into a 20 T solenoid with the velocity 90 m/sec along the solenoid axis. The density of the liquid is 1 g/cm^3, the electric conductivity is 10^{16} in Gaussian units, and the initial pressure in the liquid is 1 atm. The electrically and magnetically neutral gas outside the jet has density 0.01 g/cm and the same initial pressure. The thermodynamic properties of the ambient gas were modeled using the polytropic equation of state [4] with the ratio of specific heat $\gamma = 1.4$ and the ideal gas constant $R = 1$. The properties of the liquid jet were modeled using the stiffened polytropic equation of state with the Gruneisen exponent = 5 and the stiffened gas constant $P_\infty = 3 \cdot 10^9 g/(cm \cdot sec^2)$. The field of a magnetic coil of rectangular profile and $8 \times 8 \times 20$ cm size was calculated using exact analytical expressions.

A set of images describing the evolution of the liquid jet as it enters and leaves the solenoid is depicted in Figure 4. The strong nonuniform magnetic field near the solenoid entrance squeezes and distorts the jet. The magnetic field outside the solenoid stretches the jet which results in the jet breakup. Notice that these simulations use the expression for the current density distribution (11) which looses the quantitative accuracy when the jet is close to the breakup. Numerical results obtained using accurate numerical solutions of equation (10) are given below.

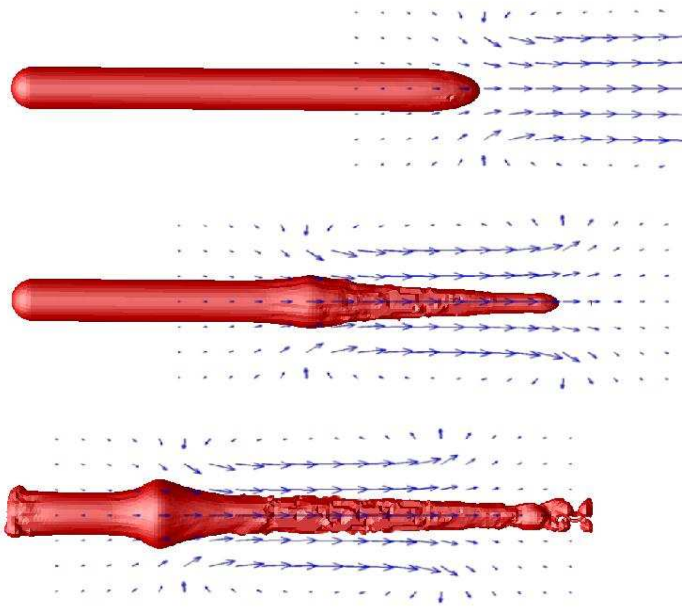

Figure 4: Liquid metal jet in a 20 T solenoid.

The numerical simulation demonstrates the influence of strong magnetic field gradients on the jet distortion. To avoid such instabilities of the mercury target during its propagation in a 20 T magnetic field, the nozzle of the mercury target was placed inside the main 20 T resistive magnetic coil (see Figure 5). Therefore the jet will not meet strong magnetic field gradients before the interaction with the proton pulses.

We have performed numerical simulations of an off-axial mercury jet moving in 20T, 15T, and 10T solenoids using accurate numerical solution for the current density distribution (see Figures 7 – 9). Our results show that the magnetic field influence will not lead to significant jet deformations. Currently, the jet is not modeled as coming form the nozzle but is initialized as a long cylinder (see Figure 6). The perturbation of the tail part of the jet (Figure 7) is caused by the nonuniform field behind the solenoid.

Interaction of mercury jet with proton pulses

Numerical simulations presented in this section aid in understanding the behavior of the target under the influence of the proton pulse, and in estimating the evolution of the pressure waves and surface instabilities. We have neglected the influence of the external magnetic field on the hydrodynamic processes driven by the proton energy deposition.

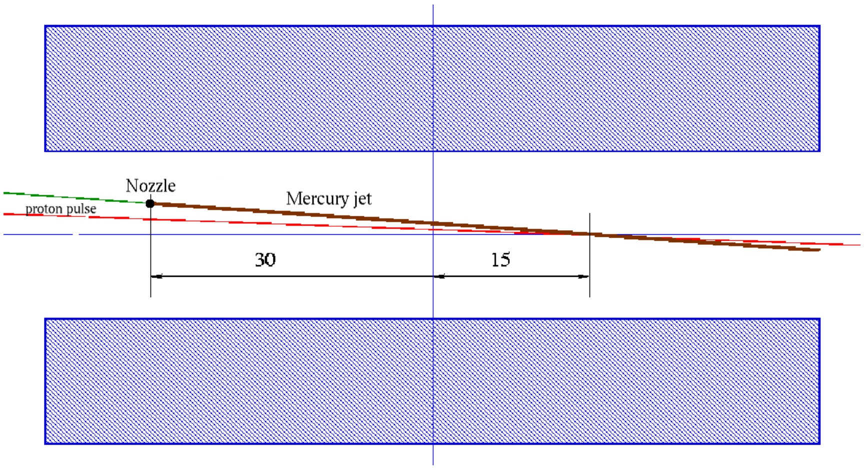

Figure 5: Schematic of the Moun Collider magnet.

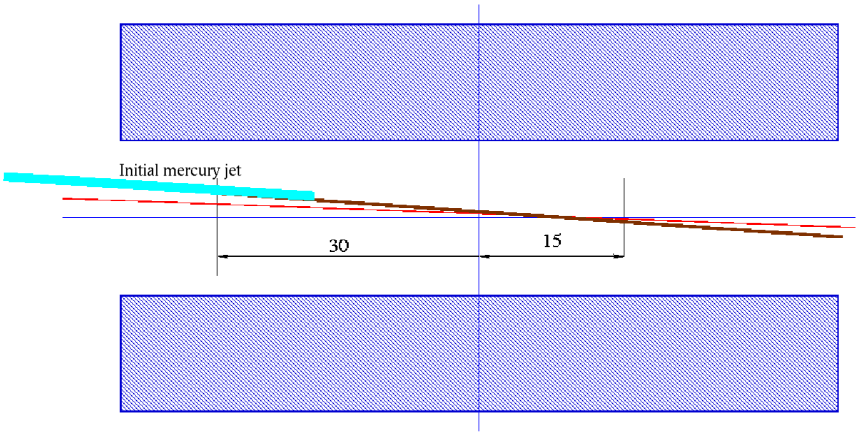

Figure 6: Initialization of the mercury jet.

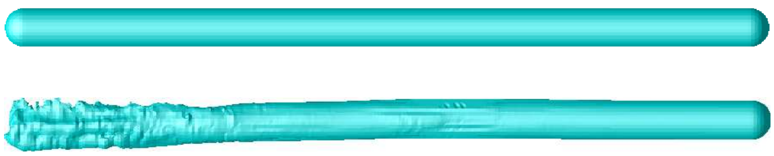

Figure 7: Evolution of the mercury target in 20T solenoid

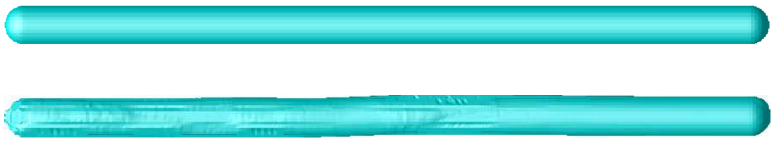

Figure 8: Evolution of the mercury target in 15T solenoid

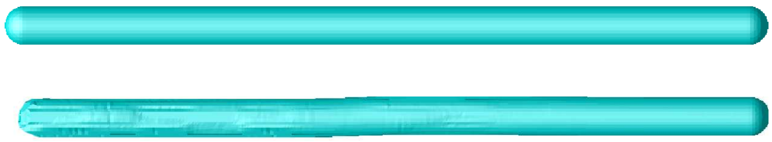

Figure 9: Evolution of the mercury target in 10T solenoid

The influence of the proton pulse was modeled by adding the proton energy density distribution to the internal energy density of mercury at a single time step. The value and spatial distribution of the proton energy was calculated using the MARS code [15]. The stiffened polytropic eos model was used for these calculations with coefficients calculated using the tabulated eos for mercury.

The evolution of the mercury target during 120 mks due to the interaction with a proton pulse is shown in Figure 10. Simulations show that velocities of surface instabilities are in the range 20 - 60 m/sec. The pressure field inside the jet developed small regions of negative pressure which indicates a possibility for the formation of cavities. Detailed studies of the cavitation phenomena in such a target will be done using the developed two-phase equation of state for mercury.

2 Proposed Research

In the future, we propoose the following research:

- Improve the robustness of the dynamic grid generator and implement new elliptic/hyperbolic solvers.
- Develop a general analytic EOS for cavitating flows.
- Numerical simulation of nozzle effects.
- Further studies of liquid metal jets in magnetic fields.
- Numerical simulation of the mercury target interacting with a high energy proton beam in the presence of a strong magnetic field.
- Numerical simulation of turbulent jets.

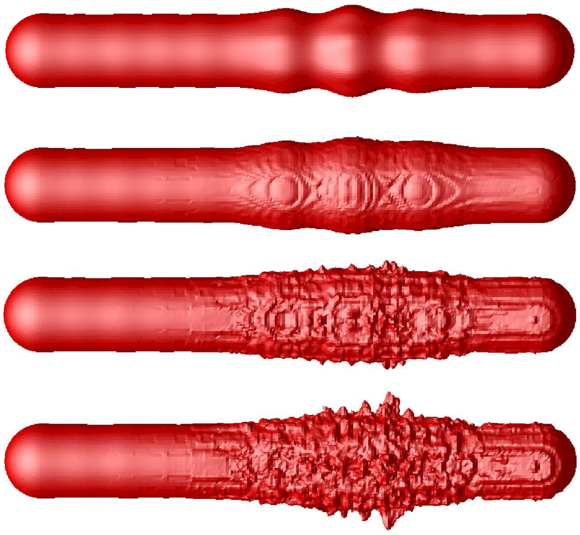

Figure 10: Evolution of the target driven by the proton energy deposition. Snapshots are shown at the initial time and 27 mksec, 78 mksec, and 120 mksec.

References

[1] Chandrasekhar, S.: Hydrodynamics and Hydrodynamic stability. Clarendon Press, Oxford (1961)

[2] G. Chavent and J. Jaffre, Mathematical Models and Finite Elements for Reservoir Simulation. North Holland, 1986.

[3] Chern, I.R., Glimm, J., McBryan, O., Plohr, B., Yaniv, S.: Front tracking for Gas Dynamics. J. Comp. Phys. **62** (1986) 83-110

[4] Courant, R., Friedrichs, K.: Supersonic Flows and Shock Waves. Interscience, New York (1948)

[5] Glimm, J., Grove, J.W., Li, X.L., Shyue, K.M., Zhang, Q., Zeng, Y.: Three dimensional front tracking. SIAM J. Sci. Comp. **19** (1998) 703-727

[6] Glimm, J., Grove, J.W., Li, X.L., Tan, D.: Robust computational algorithms for dynamic interface tracking in three dimensions. Los Alamos National Laboratory Report LA-UR-99-1780

[7] Glimm, J., Kirk, H., Li, X.L., Pinezich, J., Samulyak, R., Simos, N.: Simulation of 3D fluid jets with application to the Muon Collider target design. Advances in Fluid Mechanics III (Editors: Rahman, M., Brebbia, C.), WIT Press, Southampton Boston (2000) 191 - 200

[8] Glowinski and M. Wheeler, Domain Decomposition and Mixed Finite Element Methods for Elliptic Problems. In R. Glowinski, G. Golub, G. Meurant, and J. Periaux, Eds., Proceedings of the First International Symposium on Domain Decomposition Methods for Partial Differential Equations, pp. 144-172. SIAM, Philadelphia, 1988.

[9] K. S. Holian, T-4 handbook of material properties data bases, Vol. 1c: Equations of state, Los Alamos Report LA-10160-MS, 1984.

[10] Kirk, H., et al.: Target studies with BNL E951 at the AGS. Particles and Accelerators 2001, June 18-22 (2001) Chicago IL

[11] Landau, L.D., Lifshitz, E.M.: Electrodynamics of Continuous Media. Addison - Wesley Publishing Co., Reading Massachusetts (1960)

[12] O. McBryan, Fluids, Discontinuities and Renormalization Group Methods. In Brittin, Gustafson, and Wyss, Eds., Mathematical Physics VII, pp. 481-494. North-Holland Publishing Company, Amsterdam, 1984.

[13] Menikoff, R., Plohr, B.: The Riemann problem for fluid flow of real materials. Rev. Mod. Phys. **61** (1989) 75-130

[14] S. Balay, W. Gropp, L. McInnes and B. Smith", PETSc Users Manual, ANL-95/11 - Revision 2.1.1, Argonne National Laboratory, 2001.

[15] Ozaki, S., Palmer, R., Zisman, M., Gallardo, J. (editors) Feasibility Study- II of a Muon-Based Neutrino Source. BNL-52623 June 2001; available at http://www.cap.bnl.gov/mumu/studyii/FS2-report.html